Provided for non-commercial research and education use.
Not for reproduction, distribution or commercial use.

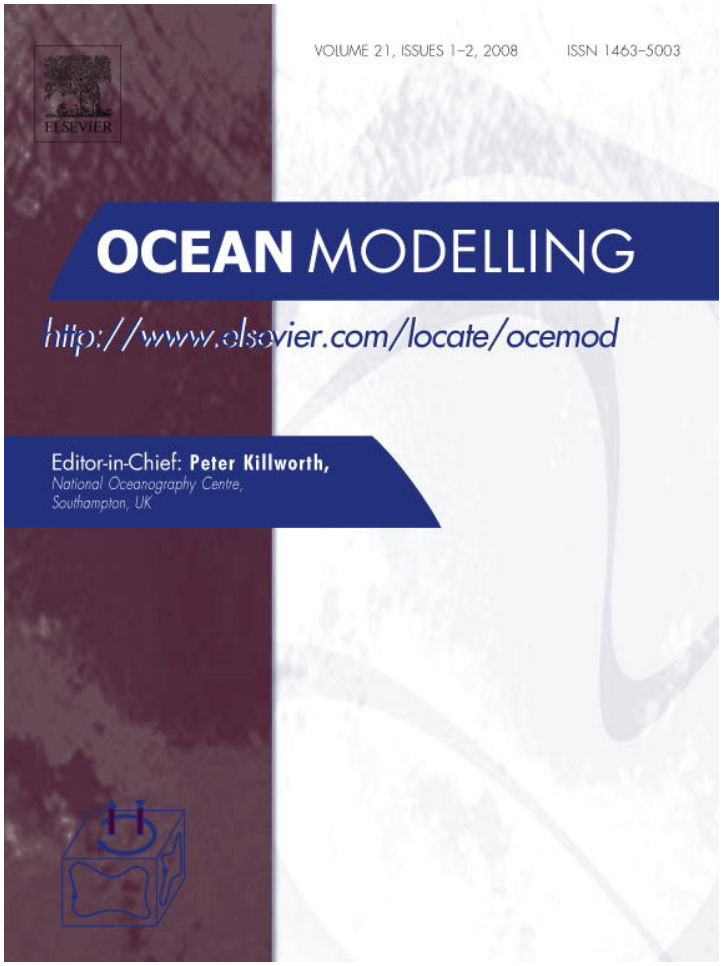

This article was published in an Elsevier journal. The attached copy is furnished to the author for non-commercial research and education use, including for instruction at the author's institution, sharing with colleagues and providing to institution administration.

Other uses, including reproduction and distribution, or selling or licensing copies, or posting to personal, institutional or third party websites are prohibited.

In most cases authors are permitted to post their version of the article (e.g. in Word or Tex form) to their personal website or institutional repository. Authors requiring further information regarding Elsevier's archiving and manuscript policies are encouraged to visit:

http://www.elsevier.com/copyright

Author's personal copy

Available online at www.sciencedirect.com
ScienceDirect
Ocean Modelling 21 (2008) 35–45
Ocean Modelling
www.elsevier.com/locate/ocemod

On transit-time distributions in unsteady circulation models

T.W.N. Haine [a,*], H. Zhang [a,1], D.W. Waugh [a], M. Holzer [b,c,d,e]

[a] Department of Earth and Planetary Sciences, 3400 North Charles Street, Johns Hopkins University, Baltimore, MD, USA
[b] Department of Applied Physics and Applied Mathematics, Columbia University, New York, NY, USA
[c] NASA Goddard Institute for Space Studies, New York, NY, USA
[d] Department of Earth and Ocean Sciences, University of British Columbia, Vancouver, BC, Canada
[e] Department of Physics, Langara College, Vancouver, BC, Canada

Received 12 June 2007; received in revised form 6 November 2007; accepted 27 November 2007
Available online 7 January 2008

Abstract

In a diffusive geophysical flow, there is not a single timescale or unique pathway for passive scalar transport from the reservoir's surface into the interior because of irreversible diffusive mixing processes. Instead, there is a range of pathways and hence a transit-time distribution (TTD) since last surface contact. We explore the issues that arise when considering TTDs for unsteady flows and discuss approaches to finding the TTD in numerical general circulation models. In particular, three complementary approaches are possible: First, the forward tracer equation can be used to simulate boundary impulse responses (BIRs). This approach is computationally efficient for the case where information on the TTD is needed at many field points or many field times. Second, the adjoint tracer equation can be used to find the TTD. This method is efficient when the TTD is required at a few field points and field times, but requires an adjoint tracer model. Third, BIR integrations can be used as statistical surrogates of TTDs, exploiting the fact that BIRs and TTDs have identical statistics due to a property of the underlying Green's function. If an estimate of the ensemble-mean TTD is required, to within an error on the order of the typical fluctuation amplitude, a single realization of the BIR serves as well as a single realization of the TTD. BIR and TTD ensembles give estimates of the ensemble-mean moments of the TTD to the same level of accuracy. Computing ensembles of BIRs instead of ensembles of TTDs is efficient for cases with few surface sources and few field times. Illustrations are presented for barotropic double-gyre circulations.
© 2007 Elsevier Ltd. All rights reserved.

Keywords: Transit-time distribution; Tracers; Circulation models

1. Introduction

Simulating dynamically-passive scalar trace substances is an important part of modern general circulation models of the ocean and atmosphere. There are many scientific reasons, including the study of radiatively-active gases and the behaviour of pollutants in the atmosphere, and biogeochemical cycling in the oceans, including the anthropogenic component of the carbon cycle. Understanding passive tracer storage and dispersal is also crucial for rotating-stratified fluid dynamics, because potential vorticity evolves as a (dynamically-active) tracer, and potential vorticity provides the dynamical foundation for many theories of the oceanic and atmospheric general circulation. Underlying all these tracer problems are common advective and diffusive transport mechanisms which determine the pathways and timescales of propagation through the fluid reservoir. Simulating these processes in circulation models is therefore a universal challenge in general circulation modelling.

Recent progress on understanding and diagnosing tracer transport has come from considering transit-time

* Corresponding author. Tel.: +1 410 516 7048; fax: +1 410 516 7933.
E-mail addresses: Thomas.Haine@jhu.edu (T.W.N. Haine), hong.zhang@caltech.edu (H. Zhang), waugh@jhu.edu (D.W. Waugh), hm2220@columbia.edu (M. Holzer).
[1] Present address: Jet Propulsion Laboratory, Pasadena, CA, United States.

1463-5003/$ - see front matter © 2007 Elsevier Ltd. All rights reserved.
doi:10.1016/j.ocemod.2007.11.004

Author's personal copy

distributions (TTDs; see, for example, Holzer and Hall, 2000, Haine and Hall, 2002, Waugh et al., 2004). The advantage of thinking about transport using TTDs is that one focuses on a revealing diagnostic that is independent of the specific source/sink characteristics of any particular tracer. The pathway and timescale information common to all tracers is readily available from the TTD.

Computing TTDs in circulation models is, in principle, a straightforward task and simply requires integration of the passive tracer equation with idealised (delta function) sources. To date, the TTDs in several models have been computed but attention has almost exclusively been on steady flow (notable exceptions are in Holzer et al. (2003), Holzer et al. (2005), Holzer and Hall (in press)). Although the general theory encompasses unsteady flow, the practical details of simulating TTDs in unsteady flow have not been explored in detail before. This issue is the main focus of our paper.

We summarise in Section 2 the basic TTD theory and explain the practical issues in computing TTDs in unsteady circulation models. Approaches using boundary impulse responses in the regular forward tracer equation and interior impulse responses in the adjoint tracer equation are compared. Each method has particular advantages and disadvantages in practice. A third approach is also possible which relies on a statistical property of the TTD and boundary impulse responses of the forward tracer equation. This property is illustrated and tested with numerical results from a barotropic, double-gyre circulation model (Sections 3 and 4). This numerical model is relatively simple yet captures the key features of mid-latitude wind-driven ocean circulations and provides a variety of flows, ranging from steady to fully chaotic regimes. Finally, we present concluding remarks in Section 5.

2. Transit-time distribution theory in unsteady flow

In an advective–diffusive geophysical flow, there is not a single timescale or unique pathway for tracer transport from the reservoir's surface into the interior because of the irreversible diffusive mixing processes. Instead, there is a range of pathways and hence a distribution of transit-times since last surface contact. Here we focus on the issues that arise when considering TTDs for unsteady flows and discuss approaches to finding the TTD in numerical circulation models. For full details on the TTD theory consult Hall and Plumb (1994), Holzer and Hall (2000) in the atmospheric context and Beining and Roether (1996), Delhez et al. (1999), Haine and Hall (2002) and Zhang et al. (2005) in the oceanic context.

2.1. Origin of the TTD

To understand the origin of the TTD consider the concentration χ of a dissolved trace species in a moving fluid. The concentration satisfies the tracer advection–diffusion equation

$$\left(\frac{\partial}{\partial t}+\mathscr{L}\right)\chi=0, \tag{1}$$

where $\mathscr{L}$ is the (linear) transport operator and includes advection and diffusion. The coefficients in $\mathscr{L}$ are considered to be known functions of space and time (typically, $\mathscr{L}(\chi)=\nabla\cdot[(\vec{u}-\mathbf{K}\cdot\nabla)\chi]$ for advecting flow $\vec{u}$ and (tensor) diffusivity $\mathbf{K}$). Appropriate boundary conditions are specified for χ at the sea floor and sea surface; typically, no flux conditions apply at the sea floor and a known (time-varying) concentration, $\chi_\Omega(t)$, applies at the sea surface, Ω (other possibilities are discussed by Haine (2006)). The solution for the tracer concentration can be written as a convolution integral

$$\chi(\vec{r},t)=\int_{-\infty}^{t}\mathscr{G}(\vec{r},t,t')\chi_\Omega(t')\mathrm{d}t'. \tag{2}$$

For simplicity we have restricted attention to a single boundary source region χ_Ω, although spatially-varying sources can also be handled with straightforward extensions (Holzer and Hall, 2000, Haine and Hall, 2002; see also (5) below). This solution (2) composes the tracer concentration $\chi(\vec{r},t)$ as a superposition of different tracer sources from different times in the past. We see that the so-called *boundary propagator*, $\mathscr{G}(\vec{r},t,t')$, propagates concentration on Ω at *source time* t' to the interior point $\vec{r}$ at *field time* t. It weights the contribution from Ω at all past times t' to the present concentration at $\vec{r}$.

The boundary propagator $\mathscr{G}$ only depends on the fluid transport from Ω to $\vec{r}$ and $\mathscr{G}$ is intimately connected to the Green's function of the transport operator (Holzer and Hall, 2000). Namely, $\mathscr{G}$ satisfies

$$\left(\frac{\partial}{\partial t}+\mathscr{L}\right)\mathscr{G}=0, \tag{3}$$

with impulsive boundary condition $\mathscr{G}(\Omega,t,t')=\delta(t-t')$ on Ω and no-flux conditions elsewhere (δ is the Dirac delta function). It contains complete information about the transport pathways and timescales in the sense that $\mathscr{G}$ contains all of the information about $\mathscr{L}$, but packaged in a different form. That is, $\mathscr{L}$($\vec{u}$ and $\mathbf{K}$) and $\mathscr{G}$ are interchangeable with each other.

For many applications the information contained in the $\mathscr{G}$ form is more useful than in the $\mathscr{L}$ form. In particular, there is a natural and revealing physical interpretation of (2). Rewriting, we see

$$\chi(\vec{r},t)=\int_{0}^{\infty}\mathscr{G}(\vec{r},t,t-\tau)\chi_\Omega(t-\tau)\mathrm{d}\tau. \tag{4}$$

Now the boundary propagator kernel is written as a function of *transit-time* (elapsed time) $\tau\equiv t-t'$. Considered from this perspective, $\mathscr{G}(\vec{r},t,t-\tau)$ weights prior boundary concentrations over transit-time and hence is called the *transit-time distribution* (TTD) for point $\vec{r}$ at time t. The TTD is the distribution of transit-times since a water parcel at point $\vec{r}$ and time t had last contact with Ω at time

Author's personal copy

$t' = t - \tau$. The quantity $\mathcal{G}(\vec{r}, t, t-\tau)\mathrm{d}\tau$ is hence the volume fraction of the parcel at $(\vec{r}, t)$ that originated from the surface Ω at a time between τ and $\tau + \mathrm{d}\tau$ ago.

Fig. 1 illustrates this idea in a schematic way by showing the boundary propagator for a particular field point as a function over source time and field time (see also Fig. 2 of Holzer et al. (2003)). The TTD corresponds to a cut through the boundary propagator in a specific direction (horizontal and to the left in Fig. 1). That is the TTD, $\mathcal{G}(\vec{r}, t, t-\tau)$, is a traverse through $\mathcal{G}$ at constant field time t, as a function of transit-time τ (and hence, source time $t-\tau$). A related, but distinct, quantity is a cut through the boundary propagator in the perpendicular direction (vertical upwards in the schematic). The vertical cut physically corresponds to the evolution with $t = t' + \tau$ of the response at interior location $\vec{r}$ to a pulse in concentration at χ_Ω that occurred during $(t', t' + \mathrm{d}t')$. This quantity, $\mathcal{G}(\vec{r}, t' + \tau, t')$, does not have an interpretation as a transit-time distribution in general: that is, it cannot be used in a formula like (2) or (4) to compose the tracer concentration by integrating over τ at fixed t'. There is no obvious name for this quantity, but we refer to it here as the boundary impulse response (BIR) because it is discussed extensively in what follows.

2.2. Steady flow

Important simplifications are possible in the case of steady flow (when $\mathscr{L}$ has no time-dependence). Then, the boundary propagator satisfies the *time-translation invariance*: $\mathcal{G}(\vec{r}, t, t-\tau) = \mathcal{G}(\vec{r}, 0, -\tau)$ for all t. This property means that the boundary propagator, and hence the TTD, only depends on the transit-time τ; only the difference between the field time and the source time (the transit-time) is relevant. In Fig. 1 this means that $\mathcal{G}$ contours are parallel to lines of constant τ and perpendicular to the $\tau' = t + t'$ lines. (Note that τ' is orthogonal to τ. In steady flow the TTD is therefore sometimes written using the shorter notation $\mathcal{G}(\vec{r}, \tau)$ for convenience. Strictly, this usage is inconsistent with the former definition, but context makes the distinction clear.) Fig. 2a illustrates the boundary propagator for the case of steady flow. On this diagram the boundary propagator is sketched as a function of source time and field time for a particular field point. For steady flow, $\mathcal{G}$ is a function of τ only, not of t' and t individually: $\mathcal{G}$ contours are parallel to lines of τ and clearly the BIR and the TTD coincide (namely, $\mathcal{G}(\vec{r}, t, t-\tau) = \mathcal{G}(\vec{r}, t' + \tau, t')$ from the time-translation invariance).

Most explicit simulations of TTDs in ocean circulation models to date have been for the case of steady flow. In practice, the TTD is found by computing the t-evolution (using (3)) of a passive tracer with an impulsive boundary concentration $\delta(t - t')$ at source time t' (often taken to be $t' = 0$ for convenience). This amounts to a vertical cut through the $\mathcal{G}$-map in Figs. 1 and 2. Formally, this approach yields the boundary impulse response which, for steady flow, equals the TTD.

2.3. Unsteady flow

In unsteady flow, some complications arise. Most important, the time-translation invariance no longer holds, implying that the TTD, $\mathcal{G}(\vec{r}, t, t-\tau)$, now depends on two independent time arguments: field time t and source time t', not just the transit-time $t - t'$. This fact means that $\mathcal{G}$-contours are no longer parallel to lines of constant transit-time (Fig. 1) and we now speak of a transit-time distribution for *each* field time and field point. Fig. 2b–d shows three distinct examples of $\mathcal{G}$ in unsteady flow: periodic flow, where a clear periodicity over field time exists,

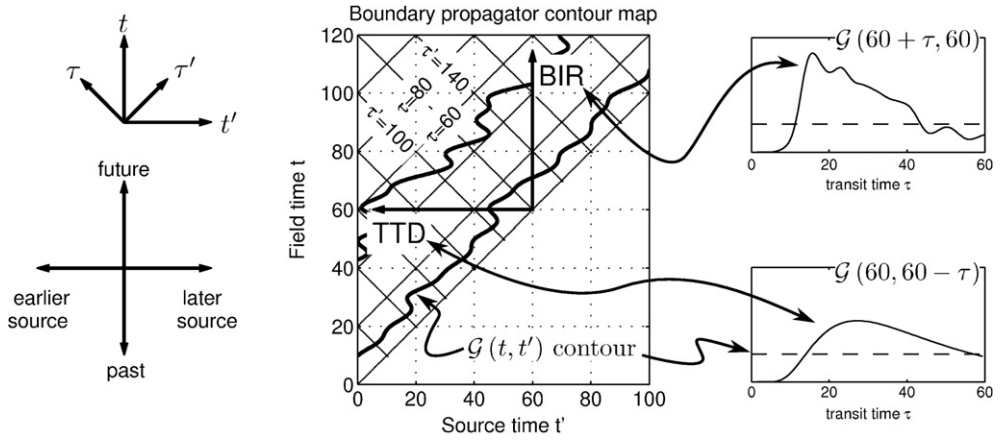

Fig. 1. Schematic diagram to explain the boundary propagator, transit-time distribution, and boundary impulse response. For a specific field point $\vec{r}$, the main panel shows two schematic contours of the boundary propagator $\mathcal{G}(\vec{r}, t, t')$ as a function of source time t' and field time t. The two contours have the same $\mathcal{G}$ value and are marked on the right hand plots with dashed lines. Because of the *causality principle*, $\mathcal{G}(\vec{r}, t, t') = 0$ for all $t' > t$, and so the lower right half of the $\mathcal{G}$-map has $\mathcal{G} = 0$ and no contours. Transit-times $\tau = t - t'$ and ortho-transit-times $\tau' = t + t'$ are also marked with diagonal lines. The transit-time distribution as a function of transit-time is $\mathcal{G}(\vec{r}, t', t' - \tau)$ and corresponds to horizontal cuts through the $\mathcal{G}$-map. The boundary impulse response is $\mathcal{G}(\vec{r}, t' + \tau, t')$ and corresponds to vertical cuts through the $\mathcal{G}$-map. In general, these two functions of transit-time are different as shown for one example in the right hand panels. For convenience, the $\vec{r}$ argument of $\mathcal{G}$ has been suppressed in the figure. See Section 2 and Fig. 2 for more details.

Author's personal copy

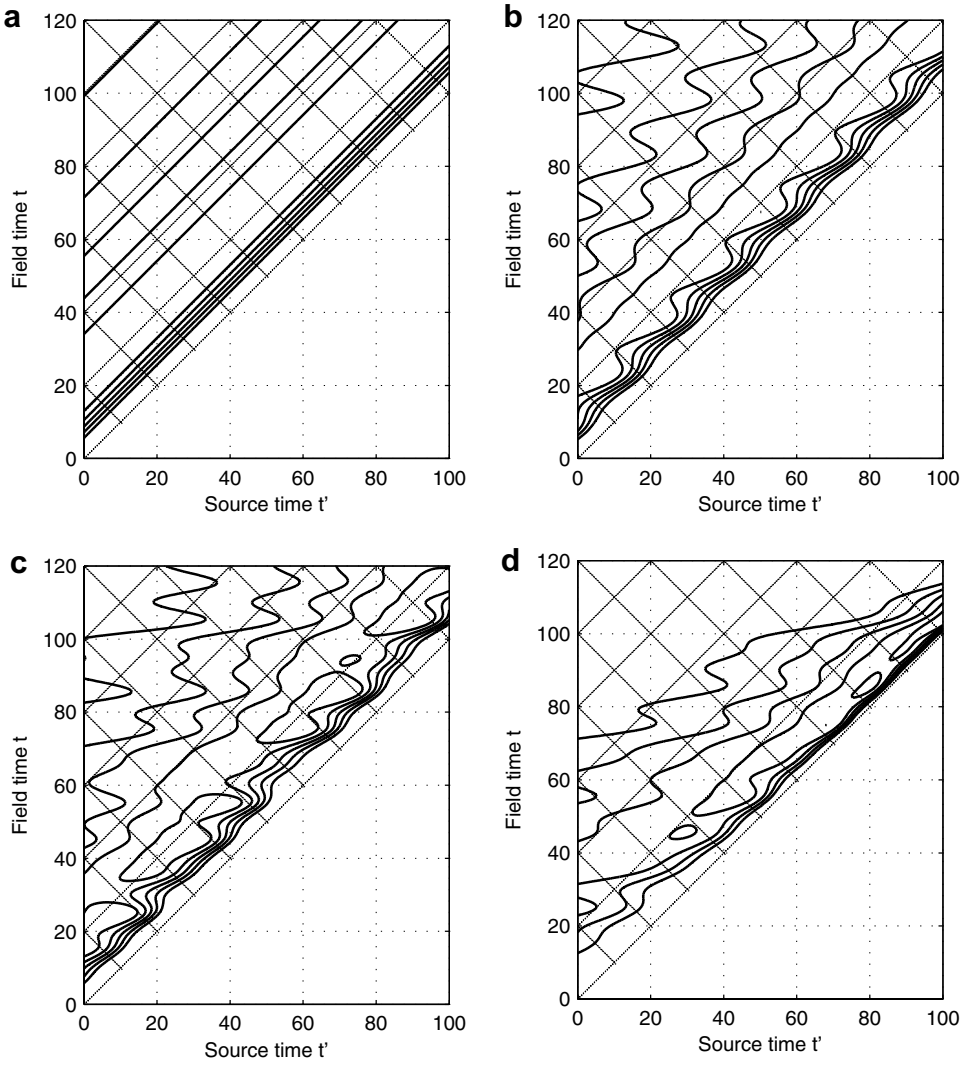

Fig. 2. Schematic diagrams of boundary propagators $\mathscr{G}(\vec{r},t,t')$ as functions of source time t' and field time t for a particular field point $\vec{r}$. (a) Steady flow, (b) periodic flow, (c) aperiodic, stationary flow, and (d) aperiodic non-stationary flow. See Section 2 and Fig. 1 for more details.

statistically-stationary unsteady flow, and non-stationary unsteady flow. We now distinguish three distinct approaches to compute the TTD, which have different advantages:

- *Method 0*: BIR from forward tracer equation. Complete knowledge of $\mathscr{G}$ requires many impulsive tracer simulations in unsteady flow. A straightforward, direct approach is to use the BIR method described in Section 2.2 and construct the $\mathscr{G}$-map by successive vertical sections. The method described by Delhez and Deleersnijder (2002) is closely related to this approach, although they use different terminology.
- *Method 1*: TTD from adjoint tracer equation. Holzer and Hall (2000) show that the TTD, $\mathscr{G}(\vec{r},t,t-\tau)$ is related to the Green's function of the adjoint tracer equation. First consider

$$\mathscr{G}(\vec{r},t,t') = \int_{\Omega} G'(\vec{r},t|\vec{r}_{\Omega},t')\,\mathrm{d}\Omega, \tag{5}$$

where $\vec{r}_{\Omega}$ is a point on the surface patch Ω and G' is the generalised form of the boundary propagator (taking surface variation of the tracer source into account). The *reciprocity relation* allows us to rewrite the integrand of (5) as follows:

$$G'(\vec{r},t|\vec{r}_{\Omega},t') = -[\mathbf{K}\cdot\nabla_{\vec{r}_{\Omega}}G^{\dagger}(\vec{r}_{\Omega},t'|\vec{r},t)]\cdot\hat{\vec{n}}, \tag{6}$$

where $\hat{\vec{n}}$ is the unit outward normal direction to the surface Ω at $\vec{r}_{\Omega}$ and $G^{\dagger}(\vec{r},t|\vec{r}_0,t')$ is the adjoint Green's function to the tracer equation (see (13) in Holzer and Hall (2000)). The adjoint Green's function satisfies (for constant fluid density)

$$\left(-\frac{\partial}{\partial t}+\mathscr{L}^{\dagger}\right)G^{\dagger} = \delta(\vec{r}-\vec{r}_0,t-t'), \tag{7}$$

subject to $G^{\dagger}(\vec{r},t|\vec{r}_0,t') = 0$ for $\vec{r}$ on Ω, and zero flux elsewhere. Put another way, one can find the TTD for a particular place and time in an unsteady flow by integrating the adjoint tracer equation (backwards) forced by an

Author's personal copy

impulsive release at the place and time of interest. The TTD is then given by the flux of adjoint Green's function leaving the domain through the surface. Delhez et al. (2004) explain a similar method to compute the residence time, which is closely related to the TTD.
This approach requires that the *adjoint* advection–diffusion system be integrated, not the forward system. While adjoint models now exist for some circulation models, they are not universally available and they are often not easy to construct.

- *Method 2*: BIR from forward tracer equation as statistical surrogate TTD. An alternative approach is available that may be advantageous in some circumstances. For example, in turbulent flows it is often more valuable to know the statistics of the TTD rather than its individual realizations. In such cases an ensemble of BIRs can be used in lieu of an ensemble of TTDs. The approach is based on BIR integrations and exploits some important statistical properties of $\mathcal{G}$ in unsteady flow. Specifically:

  For time-varying flow at point $\vec{r}$ and transit-time τ, the distribution of $\mathcal{G}(\vec{r}, t_1, t_1 - \tau)$ (the TTD) over t_1 is identical to the distribution of $\mathcal{G}(\vec{r}, t_2 + \tau, t_2)$ (the BIR) over t_2 provided that the distributions are defined over the same time intervals for t_1 and $t_2 + \tau$.

If the times t_1 and $t_2 + \tau$ for which the TTDs and BIRs are available come from different time intervals, the distributions are equal if the flow is statistically-stationary (or statistically cyclo-stationary with appropriate phasing between the two time periods). Here we consider the limit of both t_1 and t_2 ranging over all time ($-\infty$ to $+\infty$), so that the distributions of the TTDs and BIRs are always identical. The italicized equivalence above is a simple consequence of the fact that the TTD for field time t and source time $t' = t - \tau$ is identically equal to the BIR for source time t' and field time $t = t' + \tau$, namely both are equal to $\mathcal{G}(\vec{r}, t, t')$. (See the Appendix for a justification and further details; see also Holzer et al., 2003).
Roughly speaking, this statement means that for the same field point and transit-time, the TTD and BIR have identical statistics. In particular, the expected values are the same

$$\lim_{T\to\infty} \frac{1}{2T} \int_{-T}^{T} \mathcal{G}(\vec{r}, t_1, t_1 - \tau)\, \mathrm{d}t_1 = \lim_{T\to\infty} \frac{1}{2T} \int_{-T}^{T} \mathcal{G}(\vec{r}, t_2 + \tau, t_2)\, \mathrm{d}t_2. \tag{8}$$

Geometrically, one can see the reason is that these averages are taken along overlapping line segments at constant transit-time τ in the (t', t) plane (Fig. 1).
There is a minor, but important, difference between realisations of the TTD and BIR concerning normalisation: Every TTD is normalised over transit-time, $\int_0^\infty \mathcal{G}(\vec{r}, t, t - \tau)\mathrm{d}\tau = 1$ for all t (Holzer and Hall, 2000), but BIRs are only normalised over transit-time on average

$$\lim_{T\to\infty} \frac{1}{2T} \int_{-T}^{T} \int_{0}^{\infty} \mathcal{G}(\vec{r}, t' + \tau, t')\, \mathrm{d}\tau\, \mathrm{d}t' = 1, \tag{9}$$

not individually. Higher order moments of the TTD functions and the BIR functions obey similar relationships for the same reason. For example, let the mean over transit-times of the TTD be $\Gamma(\vec{r}, t) = \int_0^\infty \tau \mathcal{G}(\vec{r}, t, t - \tau)\, \mathrm{d}\tau$ and the corresponding mean over transit-times of the BIR be $\Gamma'(\vec{r}, t') = \int_0^\infty \tau \mathcal{G}(\vec{r}, t' + \tau, t')\, \mathrm{d}\tau$. Then the expected value of Γ over t equals the expected value of Γ' over t' for the same point

$$\lim_{T\to\infty} \frac{1}{2T} \int_{-T}^{T} \Gamma(\vec{r}, t)\, \mathrm{d}t = \lim_{T\to\infty} \frac{1}{2T} \int_{-T}^{T} \Gamma'(\vec{r}, t')\, \mathrm{d}t'. \tag{10}$$

Given this link between TTD and BIR statistics, one can use BIR functions from unsteady flow as statistical surrogates for the true TTD functions. The BIR functions have identical statistics to the true TTD functions, but are not actually TTDs in the sense of (4). This possibility is explored further below in a series of numerical examples.

2.4. Computational requirements

To compare and contrast these methods consider their computational requirements. Assume that we wish to represent $G'(\vec{r}, t|\vec{r}_\Omega, t')$ as a discrete matrix that is discretised with $N_{\vec{r}}$ points (or cells) over field point $\vec{r}$, N_t points over field time t, $N_{\vec{r}_\Omega}$ points over source patch $\vec{r}_\Omega$, and $N_{t'}$ points over source time t'. The storage requirements do not depend on method and are proportional to $N_{\vec{r}} N_t N_{\vec{r}_\Omega} N_{t'}$ in each case. The computer time required to compute G' does depend on method, however, as follows:

- *Method 0*: BIR from the forward tracer equation, requires $N_{t'}$ impulse response simulations over each of the $N_{\vec{r}_\Omega}$ surface patches. The resulting fields are of size $N_{\vec{r}}$ and are stored N_t times.
- *Method 1*: TTD from the adjoint tracer equation, requires N_t TTD simulations for each of the $N_{\vec{r}}$ field points of interest. The resulting fields are of size $N_{\vec{r}_\Omega}$ and are stored $N_{t'}$ times. Adjoint tracer models run slower than forward tracer models by a factor of α (typically 3–5).
- *Method 2*: The BIR as a statistical surrogate TTD, requires N_t impulse response simulations from each of the $N_{\vec{r}_\Omega}$ surface patches. The resulting fields are of size $N_{\vec{r}}$ and are stored $N_{t'}$ times. They are interpreted as TTD timeseries as explained in the preceding section.

Modern general circulation models typically have $N_{\vec{r}} = \mathrm{O}(10^{6-7}), N_{\vec{r}_\Omega} = \mathrm{O}(10^{5-6}), N_t = N_{t'} = \mathrm{O}(10^{4-6})$ if we use the model grid spacing and timestep as the appropriate discretisation for G'. The resulting G' matrix therefore has $\mathrm{O}(10^{19-25})$ elements and is obviously impossible to store, let alone compute or manipulate. Some reduction in dimension is essential either through averaging or selection of specific places and times of interest. The way this reduction is done determines the most efficient method. For example,

Author's personal copy

consider the case where a few typical TTDs are required for a few interior field points, and resolution of the TTD over surface source is not needed. Then $N_{\vec{r}} = \mathrm{O}(1)$, $N_t = \mathrm{O}(1)$, $N_{\vec{r}_\Omega} = 1$, say, and resolution of each TTD timeseries is given by $N_{t'} = \mathrm{O}(100)$ points. Method 0 then requires a time proportional to $N_{\vec{r}_\Omega} N_{t'} = \mathrm{O}(100)$, Method 1 requires a time proportional to $\alpha N_{\vec{r}} N_t = \alpha \times \mathrm{O}(1)$, and Method 2 requires a time proportional to $N_{\vec{r}_\Omega} N_t = \mathrm{O}(1)$, but gives statistical surrogate TTD timeseries with random, unbiased error. Method 1 using the adjoint tracer equation is faster than Method 0 in this case for typical α. If an adjoint tracer model is unavailable, then Method 2 offers a faster method to Method 0, but incurs error. Alternatively, if a coarsely-resolved G' for the entire model is required, we might have $N_{\vec{r}} = N_t = N_{t'} = \mathrm{O}(100)$ and $N_{\vec{r}_\Omega} = \mathrm{O}(10)$. Method 0 is then faster than Method 1 by a factor of $\alpha N_{\vec{r}} N_t / N_{\vec{r}_\Omega} N_{t'} = \alpha \times \mathrm{O}(10)$ although the computation still requires O(1000) individual BIR simulations (Holzer and Hall (in press) use this method in a tropospheric model with 15,000 tracers, for example). Method 2 is as fast as Method 0 in this case.

Other examples can be constructed to illustrate these differences. The main point is that the times required to compute G' at a given resolution scale as $N_{\vec{r}_\Omega} N_{t'}$, $\alpha N_{\vec{r}} N_t$, and $N_{\vec{r}_\Omega} N_t$ for Methods 0, 1, and 2, respectively. Moreover, each method has intrinsic disadvantages: Method 0 is likely always expensive, because resolution of the TTD in unsteady flow will presumably always require $N_{t'} = \mathrm{O}(100)$ or more; Method 1 requires an adjoint model; and, Method 2 incurs random unbiased error.

3. Numerical simulations

We numerically study these issues in idealised double-gyre circulations using the MITgcm model (Marshall et al., 1997). The main purpose of the numerical simulations is to illustrate the preceding theory and to gain some idea of typical fluctuations in TTDs, BIRs, and their moments, for a diverse range of unsteady flow regimes. The model configuration is described in a related study on tracer age and potential vorticity in unsteady flow (Zhang et al., 2005, hereinafter ZHW). Experiments are performed in a 1200 km square basin with a flat bottom at depth H on a mid-latitude β-plane. The flow starts from rest, is unstratified, and forced with a zonal wind stress, X, of the form $X = X_0 \sin(\pi y/L) f(t/T)$, where $X_0 = 0.1\ \mathrm{Nm}^{-2}$ controls the average stress amplitude, $f(t/T)$ controls the time-dependence which has a period of $T = 40$ yrs, and L is the domain size. Tracer is introduced into the model at the northern wall with source/sink characteristics to simulate the TTD and BIR as appropriate. We use a spatial grid step of 20 km and a time step of 20 min. The integration time spans 120 yrs, covering three complete forcing cycles (spin-up from rest has already occurred). For further details, see ZHW (their Section 2 and Table 1).

The tracer adjoint model is also available for the MITgcm. One view on the discretised adjoint model is to consider the sensitivity of a scalar cost function of the model state to a vector of control variables. In this context, our control variable is the initial tracer concentration at the surface and the cost function is the final tracer concentration at the particular interior point of interest. Thus we obtain the sensitivity of the tracer concentration $\chi(\vec{r}, t)$ to the prior tracer concentration at $\chi(\vec{r}_\Omega, t')$, which is just the adjoint Green's function $G^\dagger(\vec{r}_\Omega, t' | \vec{r}, t)$ required. The adjoint model propagates the sensitivity backward in time so the adjoint solutions reveal the pathways and times from which the final state arose. Typically, an adjoint calculation involves three to five times the computational cost of a forward calculation. Tests to judge the accuracy of the numerical adjoint code compared to perturbations in the forward code give agreement to machine precision (Zhang, 2005).

4. Numerical results

Four main experiments are considered: two are periodic ($H = 6000$ m) and two exhibit aperiodic (chaotic) fluctuations ($H = 2500$ m) (additional experiments are shown by Zhang (2005)).

4.1. Periodic flows

The two periodic experiments comprise a weakly forced case ($f(t/T) = 1 - 0.1 \sin 2\pi t/T$ giving a ±10% sinusoidal change in forcing) and a strongly forced case ($f(t/T) = 1 + 0.5(t/T - \lfloor t/T \rfloor)$ with a ±50% change in forcing and a sawtooth waveform; $\lfloor \cdot \rfloor$ is the floor function). TTD and BIR functions for these flows are shown in Fig. 3 (left column: weak forcing and right column: strong forcing). The top row shows that the domain-averaged kinetic energy (KE) under weak forcing oscillates at the forcing period of 40 yrs in a nearly sinusoidal manner (Fig. 3a).

Table 1
Moments from the numerical experiments

Experiment	TTD Γ (years)	BIR Γ' (years)	TTD Δ (years)	BIR Δ' (years)
Weak periodic	26.77 ± 0.19	27.05 ± 0.26	21.71 ± 0.10	21.71 ± 0.08
Strong sawtooth periodic	27.98 ± 0.82	27.18 ± 0.80	21.61 ± 0.33	21.59 ± 0.29
Weak chaotic	15.11 ± 1.59	16.25 ± 0.93	11.65 ± 0.25	11.68 ± 0.10
Strong chaotic	15.33 ± 2.24	15.36 ± 1.53	11.15 ± 0.57	11.46 ± 0.31

Results for the mean transit-time, Γ, and width, Δ, are shown for ensemble sizes of 40 TTD and 40 BIR realisations (30 each for the weak chaotic experiment). The standard deviations are also shown.

Author's personal copy

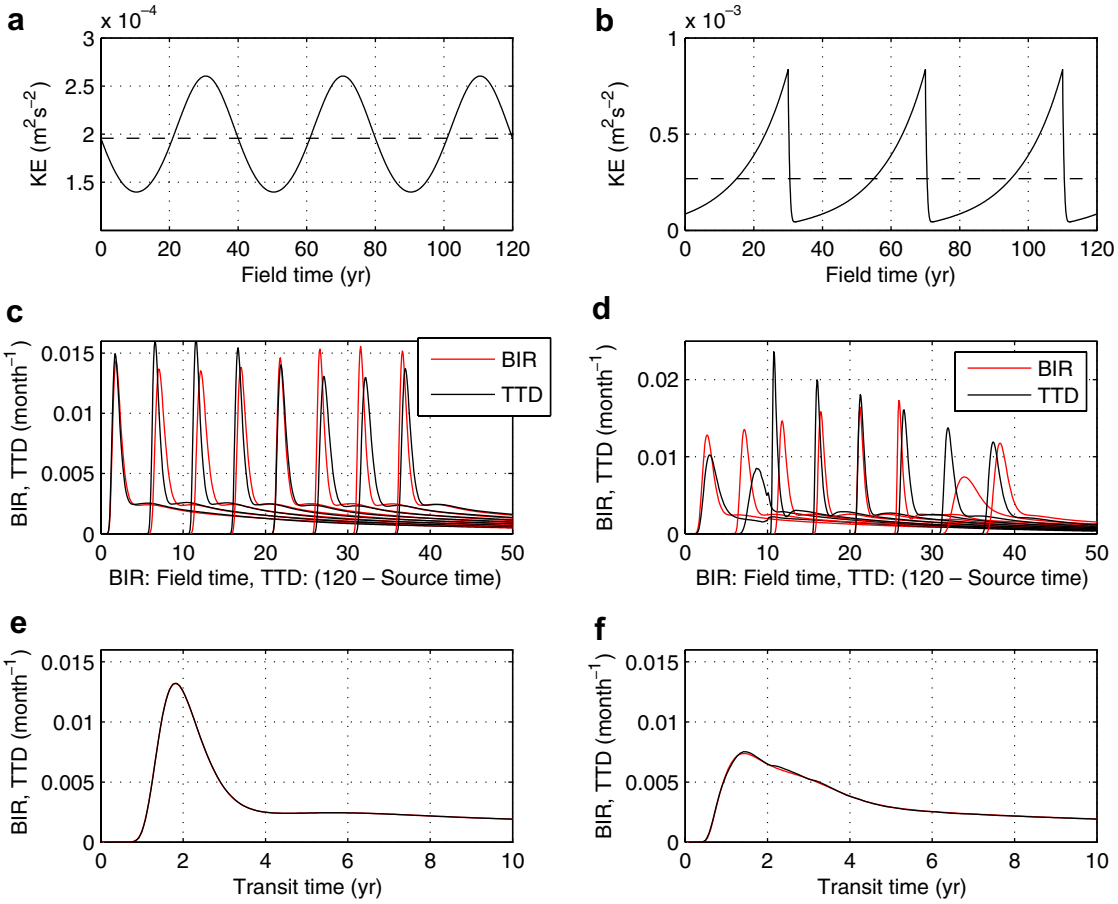

Fig. 3. TTD and BIR results for periodic experiments with weak (left) and strong fluctuations (right). (a, b) Show time series of the domain-averaged kinetic energy ($m^2\ s^{-2}$) in the model (dashed lines show the average values). (c, d) Show several realisations of the TTD (dashes) and BIR (lines) plotted against field time (yrs) for the BIR and (120-source time (yrs)) for the TTD. The source times of the realisations are separated by an interval of 5 years. (e, f) Show the ensemble average TTD (dashes) and BIR (lines) over 40 realisations plotted against transit-time. The TTD realisations are computed using the adjoint tracer model and the BIR realisations have been individually normalised for convenience. Note the different abscissa scales. See Section 4 for details.

The mean KE is $1.9 \times 10^{-4}\ m^2\ s^{-2}$, with a 30% fluctuation of amplitude (exceeding the 10% fluctuation of the wind forcing). The solid curves in Fig. 3c shows the time series of eight BIR realisations released at source times separated by 5 yrs (yr 0, yr 5, ..., yr 35) for a point at the center of the domain. For BIRs released at different times, the peak BIR values and modal times are different (high KE at source time gives an earlier, larger BIR peak). Nevertheless, the basic shape of the BIR functions is very similar.

Fig. 3 shows TTD realisations obtained by integrating the adjoint tracer model backwards over source time as described in Sections 2 and 3. Now the field times are separated by 5 years (yr 120, yr 115, ..., yr 85). The TTD patterns are very similar to the BIRs with a high, narrow first peak, a second lower, broader peak, and a long tail. Similarly, at different phases of the flow, the TTDs have different peak values and modal times. At the same phase of the flow the TTDs almost overlie the BIRs, however (for example, the first and fifth TTD and BIR functions in Fig. 3c). We also find excellent correspondence between the ensemble-mean BIR and TTD functions as shown in Fig. 3e (for 40 realisations). For this relatively weak periodic flow variation, the difference between TTD and BIR realisations taken at the same phase is almost negligible.

Fig. 3b shows the periodic oscillation of KE for the case of strong sawtooth forcing. Now the mean KE is $2.7 \times 10^{-4}\ m^2\ s^{-2}$, somewhat larger than for the weak forcing, but with higher peaks and a timeseries that is no longer symmetric under time reversal. Fig. 3d shows the BIRs (TTDs) as a function of the transit-time for eight source (field) times. As the flow slowly accelerates and gains KE, the BIR peaks become higher with reduced modal times. The corresponding TTD realisations show a similar behaviour. Near the time of rapid KE drop, the TTD and BIR functions differ significantly because of the asymmetry in flow moving forwards (BIR) or backwards (TTD) in time. Nevertheless, the ensemble averages still agree to excellent precision (Fig. 3f).

4.2. Aperiodic flow

With a water depth of $H = 2500$ m the flow enters a chaotic regime, even without time-dependent forcing. The two experiments we present here comprise a relatively

Author's personal copy

weakly-varying chaotic case ($f(t/T) = 1$) and a strongly-varying chaotic case ($f(t/T) = 1 - 0.5 \sin 2\pi t/T$).

The weakly chaotic experiment has an aperiodic KE timeseries with an average KE of 2.9×10^{-3} m^2 s^{-2}, substantially larger than the periodic cases shown above (Fig. 4a). To illustrate the circulation in this experiment, we show in Fig. 5 the mean sea-surface height and a snapshot of the same field. Clearly, the chaotic KE variations are associated with substantial disruptions of the basic double-gyre circulation and hence the transport pathways and timescales. The BIR and TTD realisations in Fig. 4c reflects these changes by exhibiting more variability than for the periodic cases. Individual realisations now have multiple peaks and there is no longer any correspondence between individual TTD and BIR functions. Fig. 4e shows the ensemble average TTD and BIR (over 30 realisations). There is good agreement between the ensemble means, as predicted by theory, but more variance than in the periodic cases.

Finally, we show in the right column of Fig. 4 the results from the strongly chaotic experiment. Now the average KE is 7.4×10^{-3} m^2 s^{-2}, larger than before. The flow is highly intermittent with sporadic periods of very high KE corresponding to highly energetic, nearly symmetric gyres that occupy the whole domain. During the intervening quiescent periods the variability resembles that found in the weakly chaotic experiment. As before, the ensemble-mean TTD and BIR functions are very similar. In fact, they are significantly closer in this experiment than for the weakly chaotic case. The TTD and BIR realisations show significant variability from case to case. Fig. 4f shows that the typical fluctuations in TTD and BIR densities are around 50–100% of the mean density near the modal transit-times, for example. The typical fluctuation is much smaller in the tails, however.

4.3. Moments

Good agreement between the ensemble-averaged TTD and BIR realisations implies agreement of the moments of these functions too. Nevertheless, it is interesting to see the exact level of agreement because in some circumstances the moments are more useful than the TTD functions themselves (ZHW). Table 1 shows results on the first two moments (mean transit-time, Γ and width, Δ; Section 2, ZHW) from the four numerical experiments. The periodic flows have very similar Γ and Δ values, but with greater variability in the strong sawtooth forcing

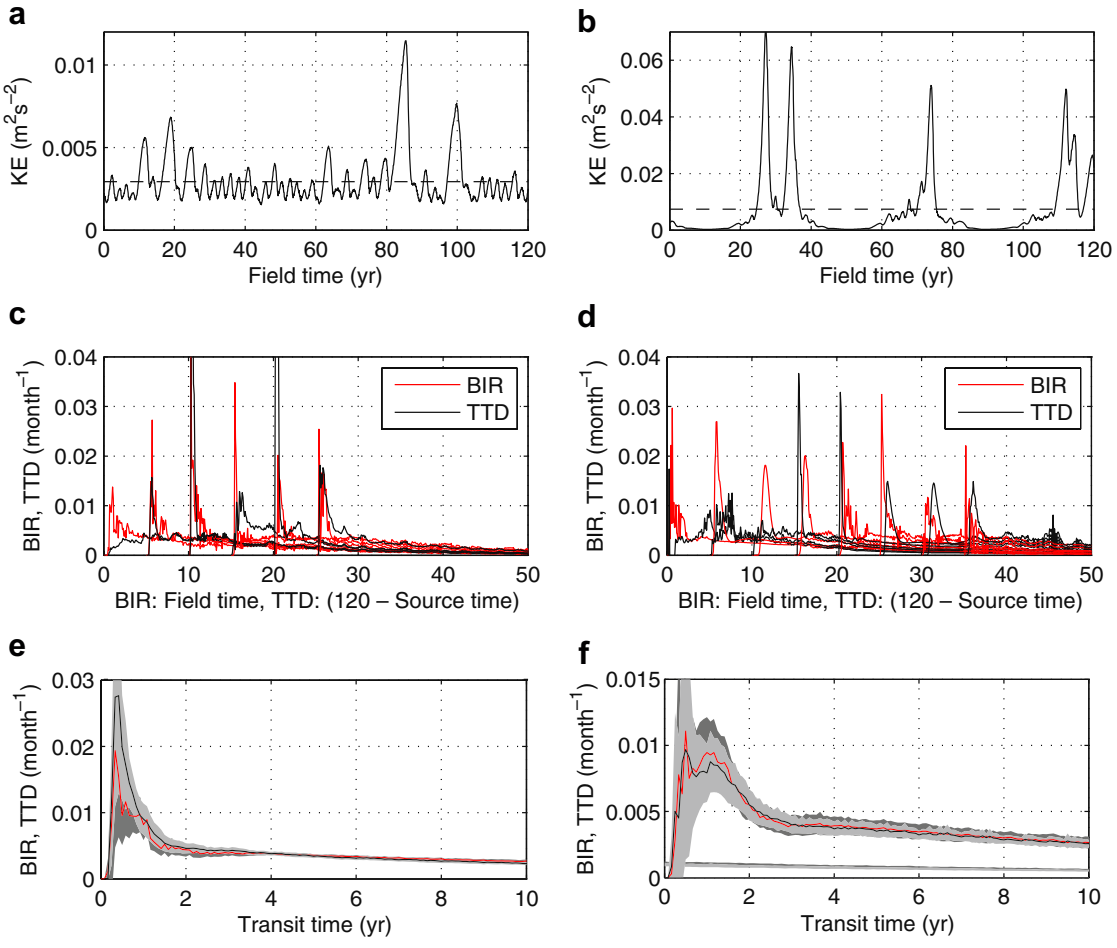

Fig. 4. As Fig 3 except for the weakly chaotic (left) and the strongly chaotic experiments (right). The shading in (e, f) indicates the range of variability (1 standard deviation) in the ensembles of BIRs (dark) and TTDs (light).

Author's personal copy

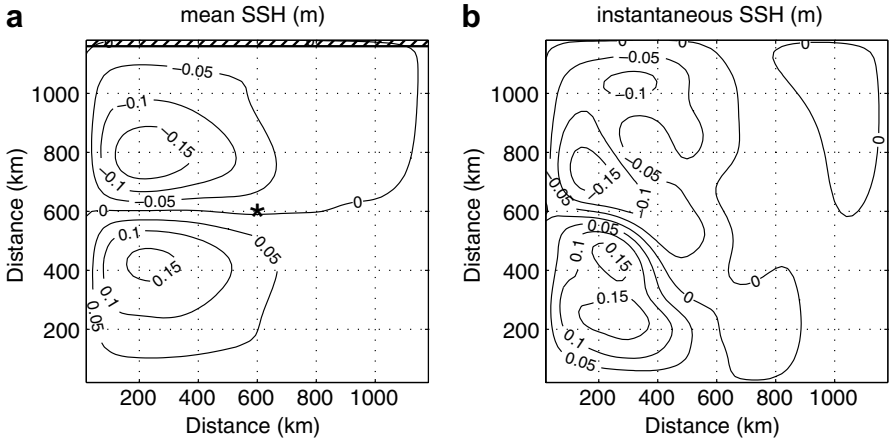

Fig. 5. (a) Time-average and (b) snapshot of sea-surface height (m) field from the weakly chaotic experiment. The hatched area is the region of tracer ventilation and the star shows where the TTD and BIR results in Figs. 3 and 4 are taken.

run. The chaotic flows have significantly smaller values of Γ and Δ, in line with the greater KE in these experiments. The variability is also larger than for the periodic flows. In all cases, the agreement between the TTD and the BIR estimates of Γ and Δ is very good. Based on the standard deviations for the strong chaotic flows shown in Table 1, the typical sampling error by which Γ and Δ differ from their ensemble-mean values is about 15% and 5%, respectively, for a single realisation. Therefore, taking a single BIR realisation as a surrogate for a single TTD realisation will give errors at this level typically. For the less energetic flows the errors are less because the circulation is both weaker (larger Γ and Δ) and less variable.

In some cases, the higher moments of the TTD are important, for example, when a tracer has a seasonal cycle in its surface source. Although convergence of higher moments is guaranteed by the theory in Section 2.3, the level of agreement seen for Γ and Δ may not apply, and convergence may be slower. Hints of this point may be seen in Fig. 4c and d, where the high-frequency TTD and BIR fluctuations (which influence higher moments) are seen to be essentially independent. If moments alone are required, rather than the full TTD, then the methods of Delhez and Deleersnijder (2002) and Zhang et al. (2005) can be employed (the Nth moment is found from a forward advection–diffusion problem and the $N-1$ lower order moments).

5. Conclusion

In this paper, we have discussed the practical issues involved in computing the transit-time distribution (TTD; G') for unsteady general circulation models. This task is relatively familiar and straightforward for steady circulations. It involves integrating an impulsive tracer using the regular forward tracer equation (called here a boundary impulse response, BIR) and then using the property that guarantees equality of the BIR and the TTD for steady flow (Section 2.2).

For unsteady flow, theory shows that the BIR and TTD are distinct quantities, however. In this case, three approaches are distinguished: First, one may determine the TTD at every field time by integrating many BIR tracers at closely spaced source times and hence scan across the entire boundary propagator as a function of source time and field time. This approach is demanding of both computer time and storage, but is relatively efficient when fine resolution of G' over field point and field time is needed (Method 0 in Section 2.3). Second, one may determine G' by integrating the adjoint tracer equation backwards as described in Section 2.3 (Method 1). This approach is relatively efficient when G' is needed for a few field points and field times, but it requires software to integrate the adjoint tracer equation which is not always available. Third, one may exploit the statistical relation between TTD realisations and BIR realisations stated in Section 2.3 (Method 2). This relation states that although the TTD and BIR functions are distinct in unsteady flow, their statistics over different realisations spanning corresponding intervals of source time and field time are identical. Thus, one can use ensembles of BIRs in lieu of ensembles of TTDs to estimate the statistical properties of the TTD. This approach is relatively efficient for cases with few field points and field times and is easy to implement.

Tests to illustrate these ideas in a simple circulation model with a wide variety of unsteady flow regimes illustrate and confirm the theory (Section 4). There is convincing agreement in the ensemble-averaged TTD and BIR functions for all experiments. Fluctuations between individual TTD and BIR realisations are typically around 50–100% near the modal times in the strongly variable flows (perhaps associated with mesoscale eddies in ocean gyres). In the tails, and for periodic flows (perhaps associated with the seasonal cycle in the upper ocean), the typical fluctuations are much smaller. When interest lies in the TTD moments, as it often does in applications concerning real observable tracers, the numerical results are encouraging. For strongly variable flow, the standard deviation

Author's personal copy

from the ensemble-mean transit-time, Γ, and TTD width, Δ, is typically around 10%. For weakly-periodic flow, the standard deviation is around 1%. The typical error incurred by swapping a single realisation of the BIR for a single realisation of the TTD is of the same order. The difference between 40-member ensemble-means was seen to be much less, as expected, because the ensemble-mean BIR and TTD must be identical in the limit of large, appropriately congruent, ensembles (Section 2.3).

These results suggest that Method 2 (BIRs as statistical surrogates of the TTDs) may achieve adequate accuracy for some applications when the difficulty or expense of the more accurate methods is a serious obstacle. Investigators should remain aware, however, that for unsteady flows BIR realisations are unequal to TTD realisations. It is straightforward to construct cases where the BIR and TTD are unrelated. For example, consider the hypothetical case where the TTD for field time t is required, and the flow changes impulsively at $t+\delta t$ (perhaps the advecting flow simply stops at time $t+\delta t$). The BIR found from a tracer release at source time t will then be unrelated to the TTD at field time t. The numerical examples in Section 4 illustrate a range of flows with oceanographic relevance, but any finite set of experiments is necessarily incomplete. If the level of agreement shown is inadequate, or the flows of interest differ substantially, then Methods 0 and 1 should be used. Nevertheless, for some purposes, where low-order moments or the ensemble-averaged TTD is required for example, Method 2 may well be satisfactory.

Acknowledgement

This work was supported by Grants from the physical oceanography program at NSF (OCE-0326670 and OCE-0136327). Comments by an anonymous reviewer helped clarify an earlier version of this paper.

Appendix. Equal TTD and BIR expectations

Here we justify the statement in Section 2 that the expectations of the TTD and BIR over transit-time are equal in unsteady flow for the same point. Statement (8) holds because of the following identity:

$$\int_{T_1}^{T_2} \mathcal{G}(\vec{r},t,t-\tau)\,\mathrm{d}t = \int_{T_1-\tau}^{T_2-\tau} \mathcal{G}(\vec{r},t'+\tau,t')\,\mathrm{d}t', \tag{11}$$

which can be seen through the simple change of variable, $t' = t-\tau$. In this equality, the left hand side is an integral over different TTDs at different field times t along a line of constant transit-time τ, and the right hand side is an integral over different BIRs at different source times t' along the same path. Letting this path extend to infinity gives the expectation of all TTDs at a fixed τ (left) and the expectation of all BIRs at the same τ (right). These expectations are equal because of (11), which implies (8).

We know from Holzer and Hall (2000) that the TTDs are normalised over transit-time ($\int_0^\infty \mathcal{G}(\vec{r},t,t-\tau)\,\mathrm{d}\tau = 1$ for all $\vec{r}$ and t), but what about the BIRs? Integrating both sides of (11) with respect to τ gives

$$\int_0^\infty \int_{T_1}^{T_2} \mathcal{G}(\vec{r},t,t-\tau)\,\mathrm{d}t\,\mathrm{d}\tau = \int_0^\infty \int_{T_1-\tau}^{T_2-\tau} \mathcal{G}(\vec{r},t'+\tau,t')\,\mathrm{d}t'\,\mathrm{d}\tau, \tag{12}$$

$$\int_{T_1}^{T_2} \int_0^\infty \mathcal{G}(\vec{r},t,t-\tau)\,\mathrm{d}\tau\,\mathrm{d}t = \int_0^\infty \int_{T_1-\tau}^{T_2-\tau} \mathcal{G}(\vec{r},t'+\tau,t')\,\mathrm{d}t'\,\mathrm{d}\tau, \tag{13}$$

$$T_2 - T_1 = \int_0^\infty \int_{T_1-\tau}^{T_2-\tau} \mathcal{G}(\vec{r},t'+\tau,t')\,\mathrm{d}t'\,\mathrm{d}\tau \tag{14}$$

$$= \int_{T_1}^{T_2} \int_0^{T_2-t'} \mathcal{G}(\vec{r},t'+\tau,t')\,\mathrm{d}\tau\,\mathrm{d}t',$$

$$\int_{-\infty}^{T_1} \int_{T_1-t'}^{T_2-t'} \mathcal{G}(\vec{r},t'+\tau,t')\,\mathrm{d}\tau\,\mathrm{d}t'. \tag{15}$$

The last step is written with the inner integral of the BIR over transit times as is needed for a BIR normalisation condition. The integration area in the (t',t) plane extends to $-\infty$ in source time, not ∞ in field time, however. Therefore, the limits of integration of the BIR over τ are not correct for the desired normalisation formula: the TTD normalisation cannot simply be manipulated into an BIR normalisation. Nevertheless, as $(T_1,T_2)\to(-,+)\infty$, the region of integration expands to fill all non-negative transit-times and we find

$$\lim_{T_1,T_2,\to\mp\infty} \frac{1}{T_2-T_1} \int_{T_1}^{T_2} \int_0^\infty \mathcal{G}(\vec{r},t'+\tau,t')\,\mathrm{d}\tau\,\mathrm{d}t' = 1, \tag{16}$$

assuming that $\mathcal{G}$ dies away with an asymptotic exponential behaviour at very large transit-times, as it must (Haine and Hall, 2002, Zhang, 2005; this kills off the second integral in (15)). Statement (16), justifying (9), says that BIRs are normalised *on average*, but individual BIR functions are not individually normalised, unlike individual TTD functions.

Average moments of the BIR and TTD satisfy similar relations to (16) for similar reasons. That is

$$\lim_{T_1,T_2,\to\mp\infty} \frac{1}{T_2-T_1} \int_{T_1}^{T_2} m_n(\vec{r},t)\,\mathrm{d}t = \lim_{T_1,T_2,\to\mp\infty} \frac{1}{T_2-T_1} \int_{T_1}^{T_2} m'_n(\vec{r},t')\,\mathrm{d}t', \tag{17}$$

where the moments of the TTD, m_n, and the BIR, m'_n, satisfy

$$m_n(\vec{r},t) = \int_0^\infty \tau^n \mathcal{G}(\vec{r},t,t-\tau)\,\mathrm{d}\tau, \tag{18}$$

$$m'_n(\vec{r},t') = \int_0^\infty \tau^n \mathcal{G}(\vec{r},t'+\tau,t')\,\mathrm{d}\tau. \tag{19}$$

Author's personal copy

The centered moments, such as the TTD width Δ, also have this property.

References

Beining, P., Roether, W., 1996. Temporal evolution of CFC 11 and CFC 12 concentrations in the ocean interior. J. Geophys. Res. 101, 16455–16464.

Delhez, E.J.M., Deleersnijder, E., 2002. The concept of age in marine modelling II. Concentration distribution function in the English Channel and North Sea. J. Mar. Syst. 31, 279–297.

Delhez, E.J.M., Campin, J.-M., Hirst, A.C., Deleersnijder, E., 1999. Toward a general theory of the age in ocean modelling. Ocean Modell. 1, 17–27.

Delhez, E.J.M., Heemink, A.W., Deleersnijder, E., 2004. Residence time in a semi-enclosed domain from the solution of an adjoint problem. Estuar. Coast Shelf Sci. 61, 691–702.

Haine, T.W.N., 2006. On tracer boundary conditions for geophysical reservoirs: how to find the boundary concentration from a mixed condition. J. Geophys. Res. 111, C05003. doi:10.1029/2005JC003215.

Haine, T.W.N., Hall, T.M., 2002. A generalized transport theory: water–mass composition and age. J. Phys. Oceanogr. 32, 1932–1946.

Hall, T.M., Plumb, R.A., 1994. Age as a diagnostic of stratospheric transport. J. Geophys. Res. 99, 1059–1070.

Holzer, M., Hall, T.M., 2000. Transit-time and tracer-age distributions in geophysical flows. J. Atmos. Sci. 57, 3539–3558.

Holzer, M., Hall, T.M., in press. Tropospheric transport climate partitioned by surface origin and transit time. J. Geophys. Res.

Holzer, M., Mckendry, I.G., Jaffe, D.A., 2003. Springtime trans-Pacific atmospheric transport from east Asia: a transit-time probability density function approach. J. Geophys. Res. 108. doi:10.1029/2003JD003558.

Holzer, M., Hall, T.M., Stull, R.B., 2005. Seasonality and weather-driven variability of transpacific transport. J. Geophys. Res. 110. doi:10.1029/2005JD006261.

Holzer, M., Hall, T.M., Stull, R.B., in press. Seasonality and weather-driven variability of transpacific transport. J. Geophys. Res.

Marshall, J., Adcroft, A., Hill, C., Perelman, L., Heisey, C., 1997. A finite-volume, incompressible Navier–Stokes model for studies of the ocean on parallel computers. J. Geophys. Res. 102, 5753–5766.

Waugh, D.W., Haine, T.W.N., Hall, T.M., 2004. Transport times and anthropogenic carbon in the subpolar North Atlantic. Deep Sea Res., Part I 51, 1475–1491.

Zhang, H., 2005. Transport timescales in ocean double-gyre circulations. Ph.D. thesis, Johns Hopkins University.

Zhang, H., Haine, T.W.N., Waugh, D.W., 2005. Relationships between tracer age and dynamical fields in double gyre circulation. J. Phys. Oceanogr. 35, 2250–2267.